Evaluating Dual-Frequency, Multi-Constellation GNSS Performance of Modern Smartphones for Atmospheric Monitoring Across Mountainous and Urban Areas

Evaluating Dual-Frequency, Multi-Constellation GNSS Performance of Modern Smartphones for Atmospheric Monitoring Across Mountainous and Urban Areas

1st Milad Bagheri
Dept. of Environment, Land and Infrastructure Engineering
Politecnico di Torino, Turin, Italy
milad.bagheri@polito.it

2nd Neil Gogoi
Dept. of Environment, Land and Infrastructure Engineering
Politecnico di Torino, Turin, Italy
neil.gogoi@polito.it

3rd Paolo Dabove
Dept. of Environment, Land and Infrastructure Engineering
Politecnico di Torino, Turin, Italy
paolo.dabove@polito.it

4th Vincenzo di Pietra
Dept. of Environment, Land and Infrastructure Engineering
Politecnico di Torino, Turin, Italy
vincenzo.dipietra@polito.it

***Abstract*—Recent advancements in Global Navigation Satellite System (GNSS) technology have enabled the integration of dual-frequency, multi-constellation capabilities into modern smartphones, significantly enhancing their potential for various applications beyond traditional navigation. One promising application is atmospheric monitoring, where GNSS-based observations—such as those of atmospheric water vapor—are used to improve weather forecasting, track climatic changes, and provide critical insights for environmental studies. However, the use of smartphones for GNSS-based atmospheric monitoring faces challenges, particularly in terms of signal reliability and accuracy, which can vary significantly depending on the surrounding environment. The authors aim to evaluate the performance of dual-frequency, multi-constellation GNSS capabilities in modern smartphones for atmospheric monitoring across both urban and rural environments, providing a comprehensive analysis of their accuracy, reliability, and potential limitations. Towards that, this paper presents a preliminary study on the feasibility of estimating the Zenith Tropospheric Delay at different environments and elevation through the collection of GNSS data from a flagship high-end Android smartphone equipped with dual-frequency (L1 and L5) and multi-constellation (GPS, Galileo, GLONASS, and BeiDou) capabilities and pitching it against a high performing commercial low-cost GNSS receiver. Preliminary results suggest that modern smartphones equipped with dual-frequency, multi-constellation GNSS are capable of promising accuracy for atmospheric monitoring, particularly in rural or high elevation areas with minimal obstructions. Our findings indicate that such smartphones have the potential to serve as low-cost, accessible tools for atmospheric monitoring, especially in open-sky rural environments where conditions are more favorable.**

***Index Terms*—GNSS dual-frequency, smartphone positioning, atmospheric monitoring, challenging areas, urban environment**

I. Introduction

The Earth's atmosphere is a complex system that affects weather patterns, climate variability, and geophysical processes. Accurate monitoring of atmospheric changes is crucial for enhancing numerical weather models (NWMs), predicting extreme weather events, and comprehending long-term climate patterns. A highly effective method to accomplish this is through Global Navigation Satellite System (GNSS) meteorology, which utilizes GNSS signals to determine tropospheric properties, including Zenith Tropospheric Delay (ZTD). The propagation of GNSS signals is influenced by atmospheric refractivity; thus, accurate prediction of ZTD yields essential insights into water vapor distribution, which is essential for meteorological and climate research.

Traditionally, geodetic-grade GNSS receivers have served as the benchmark for tropospheric monitoring, providing high-precision measurements that fulfill the demands of meteorological applications. These high-performance receivers are utilized in national or regional networks such as the International GNSS Service (IGS) [1], the EUREF Permanent Network (EPN) [2], and the SPIN3 interregional positioning service [3]. Nonetheless, their high expense and limited availability present considerable obstacles, especially in underdeveloped areas where extensive GNSS networks are financially impractical. This constrains the use of GNSS meteorology in global atmospheric research, particularly in regions deficient in comprehensive observational infrastructure. To address this challenge, low-cost GNSS devices emerged as a feasible option, as evidenced by numerous recent studies. Studies indicate that low-cost GNSS receivers, when paired with suitable antennas, can estimate Zenith Tropospheric Delay (ZTD) with precision comparable to geodetic-grade receivers [4]. Subsequent investigations have confirmed the efficacy of low-cost receivers for climate monitoring, revealing a significant correlation between GNSS-derived ZTD and ERA5 reanalysis data, hence substantiating their applicability in atmospheric studies [5]. Improvements in receiver technology and antenna

calibration have enhanced the quality of tropospheric estimates obtained from dual-frequency low-cost GNSS devices, rendering them more competitive with geodetic-grade solutions [6]. Additionally, the viability of low-cost GNSS networks for atmospheric monitoring has been investigated, with studies indicating that these networks can deliver continuous and high-resolution tropospheric delay measurements [7]. Networks such as Centipede RTK have been examined as alternatives for regional meteorological applications, emphasizing the possibility of distributed low-cost GNSS solutions in enhancing tropospheric monitoring capabilities. The scalability and cost-effectiveness of these networks render them a viable solution for enhancing GNSS meteorology in areas where the installation of advanced equipment is economically impractical.

The growing viability of low-cost GNSS networks has created new potential for enhancing tropospheric monitoring through the establishment of denser and more economical observational networks. The integration of GNSS-enabled smartphones into atmospheric monitoring frameworks represents a significant achievement in this field. Billions of smartphones with GNSS receivers globally provide a widely accessible, distributed sensor network that might substantially improve regional and global atmospheric observations. Taking advantage of this accessibility, the potential of using a large distributed network of smartphones as a powerful scientific instrument for monitoring the ionosphere is demonstrated in [11]. A similar effort used crowdsourced smartphone GNSS data towards high-precision ZTD determination with certain limitations [12].

A plethora of studies recently assessed the performance of ultra-low-cost GNSS chip-sets integrated into smartphones, examining their hardware performances [13], [14], raw measurement profiles [15]–[17] and positioning performances with novel approaches across various models [18], [19]. Initially developed for navigation purposes, smartphone GNSS has evolved through advancements in multi-frequency GNSS chipsets, raw data accessibility, and post-processing methodologies, revealing its capabilities for high-precision geodetic and meteorological applications. Since the introduction of Android Nougat in 2016, smartphones have acquired the capacity to access raw GNSS measurements, generating considerable academic interest in smartphone-based GNSS positioning [8]. The cost-efficiency and extensive accessibility of GNSS-enabled smartphones have facilitated their use in many domains, such as cadastral surveys, mapping, and pedestrian navigation. Nonetheless, issues persist, especially regarding noisy observations, ambient influences, and smartphone holding configurations, which impact the accuracy of smartphone GNSS positioning [8]. Despite these limitations, research has shown that centimeter-level positioning is achievable with smartphone GNSS, especially when utilizing carrier-phase measurements [9]. Research has identified the smartphone's antenna as a critical limiting element, contributing to multipath effects and time-correlated phase errors that affect the resolution of integer ambiguities [9]. Nonetheless, advancements in GNSS chipset design and multi-frequency tracking have reduced certain constraints, hence improving smartphone positioning efficacy. The introduction of dual-frequency GNSS chipsets in smartphones has significantly enhanced their capabilities, especially in PPP applications. Studies indicate that dual-frequency PPP utilizing smartphone GNSS can get sub-meter precision under favorable conditions and approach the efficacy of single-frequency geodetic receivers [10]. A study assessing the Xiaomi Mi 8 in static and kinematic PPP modes revealed that post-convergence, RMS positional errors were 21.8 cm (E), 4.1 cm (N), and 11.0 cm (U) [10]. Furthermore, real-time GNSS correction services, such as the Galileo High Accuracy Service (HAS), have been assessed for their efficacy in improving GNSS positioning, including smartphones, especially in pedestrian applications [20]. Research demonstrates that HAS can diminish horizontal positioning inaccuracies to under 20 cm, enhancing reliability in both static and kinematic environments.

II. Experimental Setup and Methodology

A. Selection of Test Sites

To assess the performance of GNSS-based tropospheric delay estimate utilizing smartphones, experiments were performed in two distinct environments:

- Mountainous Environment (High Altitude, open sky): The initial testing location was Torgnon Ski Resort, situated in the Aosta Valley region of Northern Italy. This elevated site features reduced air pressure, difficult topography, and possible multipath interference from adjacent mountains. Performing GNSS observations in this environment facilitates the evaluation of tropospheric delay fluctuations and signal performance in high altitudes. A 15-minute static test and a 10-minute kinematic test were performed at this site. This location is referred to as Test Site 1 in this paper.

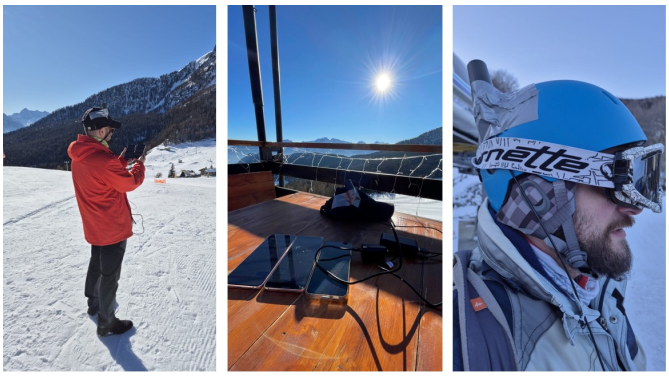

Fig. 1. Images from a mountainous setting, high altitude open sky testing area. The right shot illustrates the attachment of the Emlid mini GNSS antenna to the professional skier's helmet for kinematic testing.

- Urban Environment (Low Altitude): The second test site was at Politecnico di Torino in Turin, Italy, located at the center of the city, demonstrating a low-altitude urban environment. This environment is defined by a multipath interference and signal blockages due to urban

structures. GNSS-based tropospheric research in urban and semi-urban environments elucidates the impact of atmospheric and urban variables on GNSS signal integrity and ZTD estimation. A 15-minute static test and a 15-minute kinematic test were performed at this site. This location is referred to as Test Site 2 in this paper.

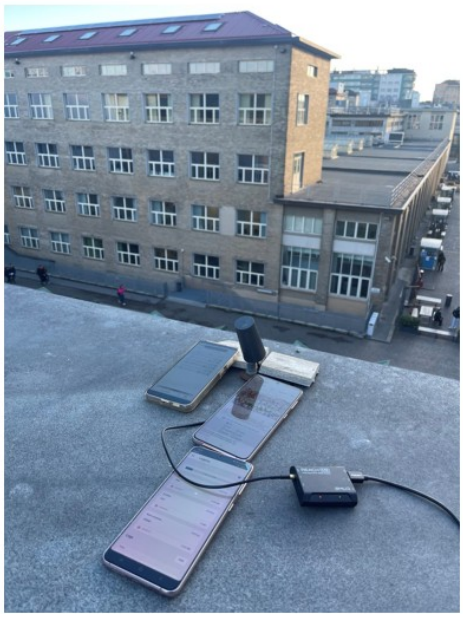

Fig. 2. Urban environment low altitude. Rooftop of DIATI department at Politecnico di Torino (Italy).

While most studies assessing ZTD accuracy typically use data collected over hours or days, the intent here was to evaluate the viability of PPP and ZTD estimation using short observation windows (15 minutes) to reflect more realistic, user-level usage scenarios of smartphones in instantaneous or near real-time applications. The quality of the raw measurements was not sufficient for kinematic tests; therefore, this study focuses exclusively on the results from static test sessions.

B. Experimental Setup and Hardware

The research employed a modern-day flagship smartphone alongside an economical GNSS receiver to evaluate the viability of the ZTD estimate in various situations and to compare the performance of the smartphone with that of the low-cost GNSS receiver. The Samsung Galaxy S24 smartphone includes a dual-frequency multi-GNSS processor with the capacity to capture raw GNSS observations, and due to its recent release, it represents the standard modern smartphone technology. This smartphone is a commercially available, mass-market device with potential uses in atmospheric monitoring. An Emlid Reach M2 GNSS receiver with its standard Multi-band GNSS antenna was utilized as an economical GNSS option together with the smartphone. The Emlid Reach M2 was chosen for its capacity to conduct multi-frequency GNSS observations while being cost-effective and readily available. The smartphone and the Emlid Reach M2 are referred to as SM and ER, respectively, in the analysis. A geodetic-grade GNSS antenna and receiver were not employed for the primary performance comparison, as the objective of this study was to assess the feasibility of atmospheric monitoring using the ultra low-cost GNSS hardware in a smartphone to high performing low-cost mass-market devices such as the Emlid Reach M2.

Fig. 3. GNSS receivers used in the tests, A) Emlid reach M2 GNSS receiver + Multi-band GNSS antenna and B) Smartphone Samsung Galaxy S24.

All devices were configured to collect multi-constellation GNSS observations (GPS and Galileo) in both static and kinematic modes at both test sites. For the smartphone, raw GNSS data was recorded using the GnssLogger application, an open-source tool developed by Google™ for capturing and exporting raw GNSS measurements from Android devices from the smartphone Application Programming Interface (API). The application enables the logging of measurements such as pseudorange, carrier-phase, Doppler, satellite signal strengths, etc., providing essential data for post-processing and precise positioning algorithms. It also processes out the data in the standard Receiver Independent Exchange (RINEX) format. Geo++ RINEX Logger developed by Geo++™ was also explored to collect the RINEX measurements, but there was a software problem with the smartphone, and it logged only a fraction of the measurements during the tests.

The recorded RINEX data from the GNSSLogger application was used to facilitate post-processing and ZTD estimation. The RINEX files were preprocessed to enable ZTD calculation and Precise Point Positioning (PPP). To facilitate a thorough and generalized study, two separate software packages were utilized, each with unique processing configurations. The initial software employed was RTKLIB, an open-source post-processing tool (available at https://www.rtklib.com/). RTKLIB offers a versatile and interactive analytical framework, enabling precise adjustment of PPP processing parameters to get tropospheric delays and positioning solutions. The second software utilized was the Canadian Spatial Reference System (CSRS-PPP), an online post-processing service (available at https://webapp.csrs-scrs.nrcan-rncan.gc.ca/geod/tools-outils/ppp.php). CSRS-PPP is acknowledged for providing exceptionally precise PPP solutions, with ZTD values closely aligning with those of the International GNSS Service (IGS) within an approximate margin of 1 cm. The utilization of

these two separate software programs guarantees a rigorous validation of the estimated tropospheric delays and positioning results.The main characteristics and processing settings used for each software are summarized in Table I. Both RTKLIB and CSRS-PPP implement Precise Point Positioning (PPP) algorithms using ionosphere-free combinations of dual-frequency code and carrier-phase GNSS observations. This combination eliminates the first-order ionospheric delay and the Iono-free Pseudorange P_{IF} and Carrier Phase L_{IF} observables are derived as the following equations:

$$P_{IF} = \frac{f_1^2 P_1 - f_2^2 P_2}{f_1^2 - f_2^2}, \quad L_{IF} = \frac{f_1^2 L_1 - f_2^2 L_2}{f_1^2 - f_2^2} \tag{1}$$

where P_1, P_2 and L_1, L_2 are pseudorange and carrier-phase observations on L1 and L2 frequencies, and f_1, f_2 are the respective frequencies. The PPP algorithm estimates the receiver position, clock bias, phase ambiguities, and Zenith Tropospheric Delay (ZTD). The tropospheric delay, $T_{r,s}$ is modeled as:

$$T_{r,s} = m_h(El) \cdot ZHD + m_w(El) \cdot (ZTD - ZHD) \tag{2}$$

where $m_h(El)$ and $m_w(El)$ are hydrostatic and wet mapping functions depending on the satellite elevation angle El, and ZHD is the Zenith Hydrostatic Delay, typically computed using the Saastamoinen model. RTKLIB applies the Niell Mapping Function (NMF), while CSRS-PPP uses the Global Mapping Function (GMF). Both tools use precise satellite clock and orbit corrections and differ slightly in constellation support and processing models, as summarized below:

TABLE I
SOFTWARE CAPABILITIES USED IN THIS STUDY.

Software	Ver.	Constell.	Freq.	Obs.	Cut-off	Mapping
RTKLIB	demo5	GPS, GLO, GAL	L1, L2	C+P	10°	NMF
CSRS-PPP	4	GPS, GLO	L1, L2	C+P	7.5°	GMF

Note: C+P = Code + Phase; GAL = Galileo; GLO = GLONASS; NMF = Niell Mapping Function; GMF = Global Mapping Function.

It is important to note that the intent was not to directly compare the performance of CSRS-PPP and RTKLIB, as they differ in supported constellations and ambiguity resolution strategies. Instead, both tools were employed to validate the consistency and robustness of ZTD estimation results independently of the software used. For the static positioning reference, the TNUS GNSS master station, located around 10 kilometers from the test area, was used to obtain the reference solution in relative mode. The GNSS raw measurements were post-processed using RTKPOST, a module of RTKLIB, to achieve high-precision positioning with a standard deviation of only a few millimeters. This geodetic reference solution allowed for a rigorous evaluation of the smartphone and low-cost GNSS receivers' performance, ensuring a reliable benchmark for positioning accuracy. The combination of PPP-based absolute positioning and high-precision relative positioning using a nearby geodetic master station enables a comprehensive assessment of tropospheric delay estimation and positioning performance across different GNSS receiver types.

III. Results and Discussion

A. High Altitude Open Sky Tests

The skyplot of GPS and Galileo satellites on the 17th of January, 2025, at the test site Fig. 4. SM is seen to have a higher availability of satellites, with the difference being more number of Galileo satellites being tracked by its receiver. The difference in quality of the measurements, however, is stark, as seen later in this section. The combined GPS and Galileo satellite availability for both L1 and L5 frequencies can be seen in Fig. 5, and the difference in continuity between the two receivers is seen. There are sufficient satellites to perform RTK and PPP positioning as required by this work.

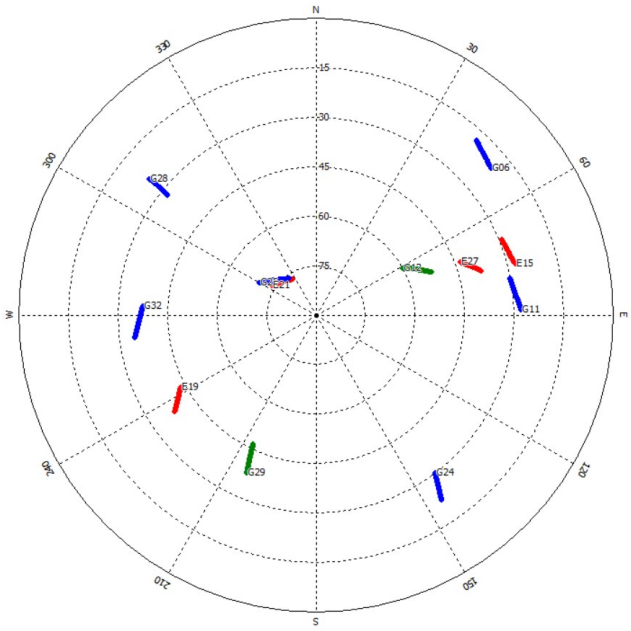

Fig. 4. Skyplot of High Altitude Test Site 1

1) Analysis of GNSS Raw Measurements: The quality of the GPS L1 pseudoranges of SM and ER for a higher and lower elevation satellite, Space Vehicle Identifier (SvID) 25 and 28, respectively, in a static test environment can be seen in Fig. 6 obtained via detrending the measurements to visualize the noise in the code measurements. For short time spans, detrended pseudorange measurements could be considered as an ergodic process, and were obtained through second-order differentiation [15], [21]. Similarly, Galileo SvID 21 and SvID 15 were selected as the higher and lower elevated satellite, respectively, and the noise profile is similar in their code pseudorange measurements as seen in Fig. 7. It is seen that

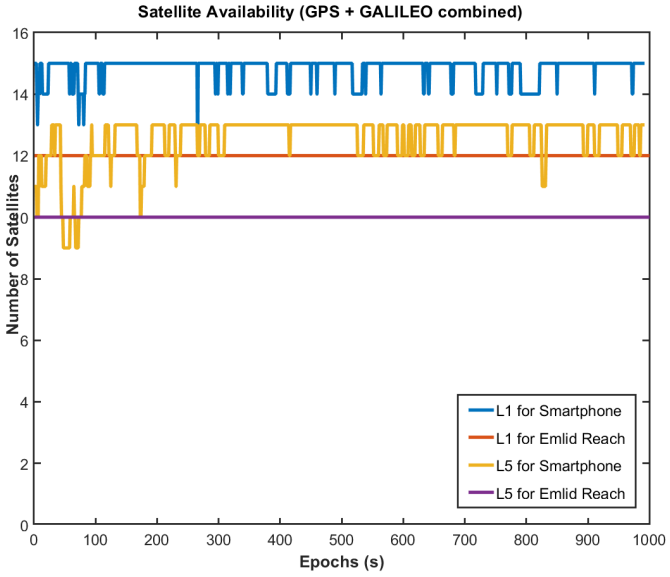

Fig. 5. Combined Satellite Availability at Test Site 1

the code pseudorange quality of L5 measurements for both constellations were of similar profile.

The quality of the carrier phase measurements for the same pair of GPS and Galileo satellites can be seen in Fig. 8 and Fig. 9. The difference in availability and continuity of carrier phase measurements is in stark contrast between the SM and ER. It displays the improbability of using carrier phase measurements in positioning and related algorithms for the modern-day smartphone. There is 100% availability of carrier phase measurements in the ER, however there are 5 peculiar cycle slips which occur across the 15 minute observation period. They appear in all satellites across GPS and Galileo for both L1 and L5 frequencies. The Signal-to-Noise Ratio (SNR) measurements for the selected satellites can be seen in Fig. 10 and Fig. 11 and the lack of an SNR disturbance to the ER during these 5 epochs suggest that the cycle slips are not due to external interference, rather probably due to the internal receiver hardware or software. The SNR plots also highlight the difference between an omnidirectional smartphone planar inverted-F or patch antenna and a standard commercial GNSS antenna. The SNRs for L5 measurements were around 5 dB-Hz lower in the SM and around 2 dB-Hz higher for the ER for both constellations when compared to L1.

Table. II denotes the availability of carrier phase measurements as a percentage during the test duration and the number of cycle slips that have occurred during that period for both frequencies and selected SvIDs. It further highlights the difference in the availability of carrier phase measurements between SM and ER, and the number of cycle slips in the measurements is computed to further drive the point that traditional carrier phase-based positioning algorithms are improbable with the SM. It also shows that except for the seen internal disturbances affecting all satellites, there is full availability of carrier phase measurements for the ER, even for the lower elevated satellites.

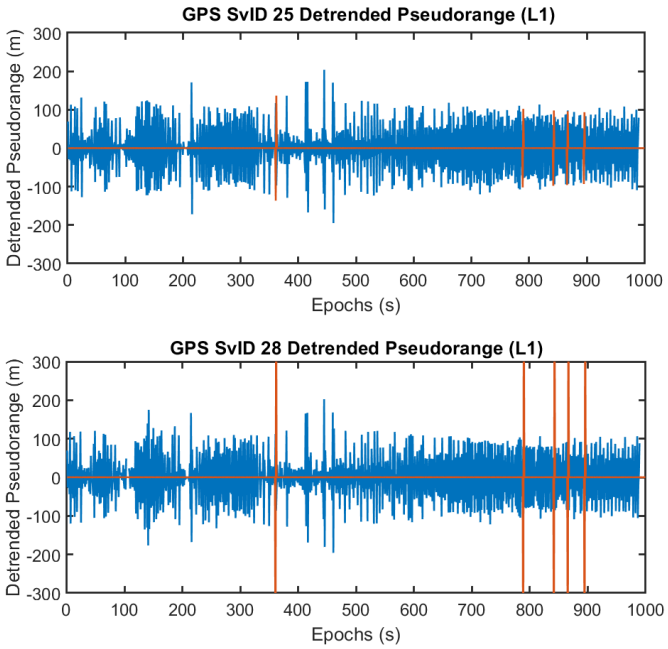

Fig. 6. GPS L1 Code Pseudorange Comparison for Test Site 1

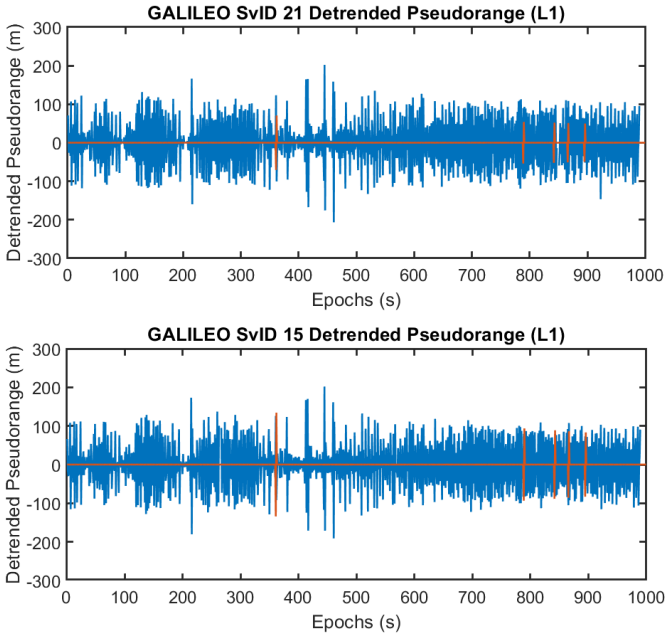

Fig. 7. Galileo L1 Code Pseudorange Comparison for Test Site 1

2) Post Processed Positioning and ZTD Estimation Performances: To guarantee a comprehensive assessment of the PPP performance, two distinct software platforms, RTKLIB and CSRS-PPP, were employed for post-processing. This dual-software strategy improves the dependability and generalization of the outcomes by utilizing several approaches and configurations in processing. The comparative study of these

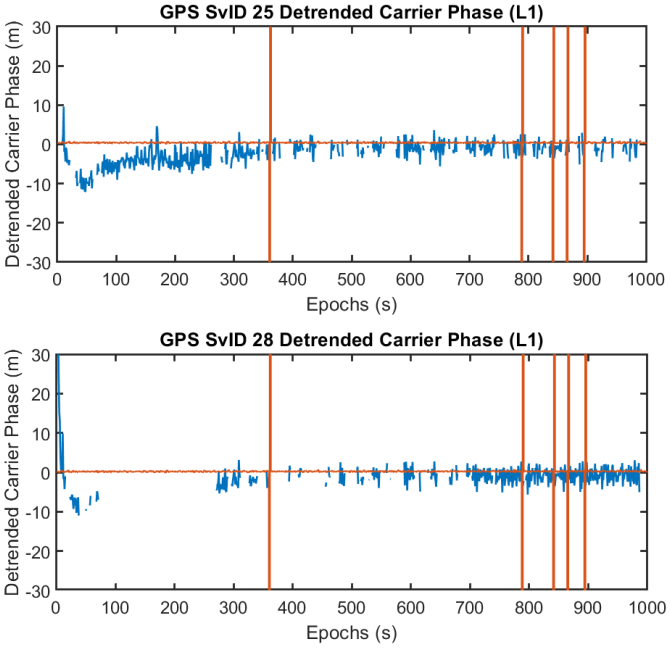

Fig. 8. GPS L1 Carrier Phase Comparison for Test Site 1

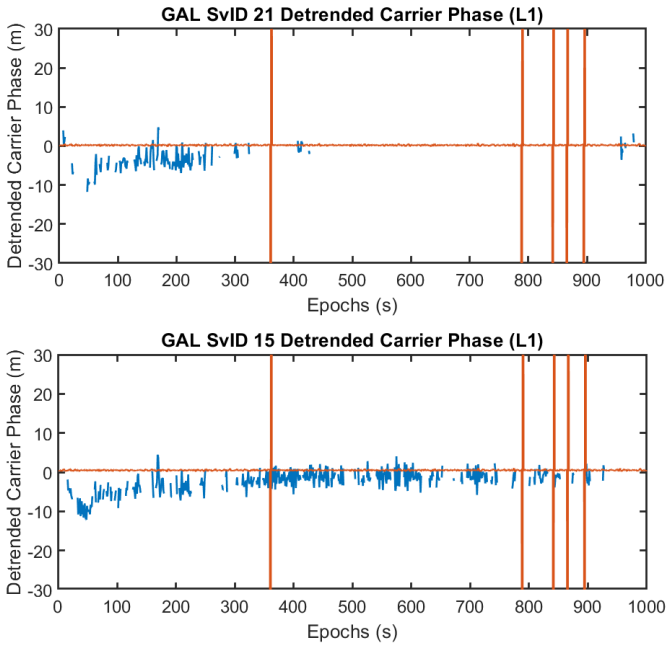

Fig. 9. Galileo L1 Carrier Phase Comparison for Test Site 1

tools is essential for evaluating positioning accuracy and ZTD estimations, especially when contrasting hardware platforms like the low-cost Emlid Reach M2 GNSS receiver and the smartphone Samsung Galaxy S24.

The reference solution was derived by post-processing the GNSS raw measurements in relative mode utilizing the TNUS GNSS master station within the SPIN3 GNSS network. This geodetic-grade reference established a benchmark with a millimeter-scale standard deviation, facilitating a thorough

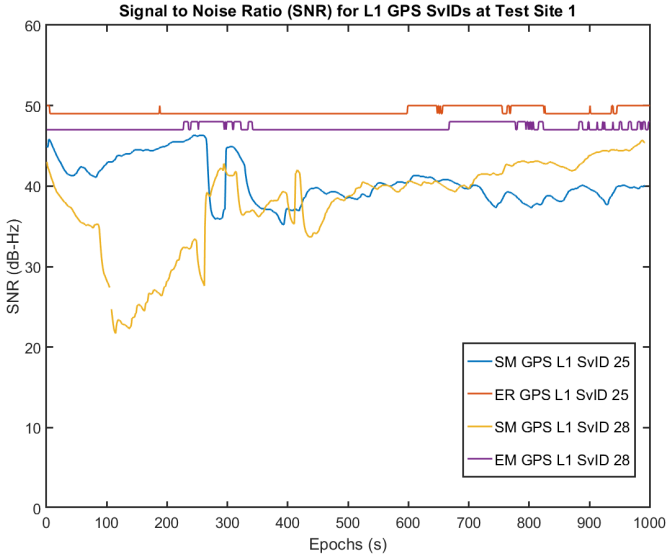

Fig. 10. Signal-to-Noise Ratio of selected L1 GPS SvIDs for both receivers at Test Site 1

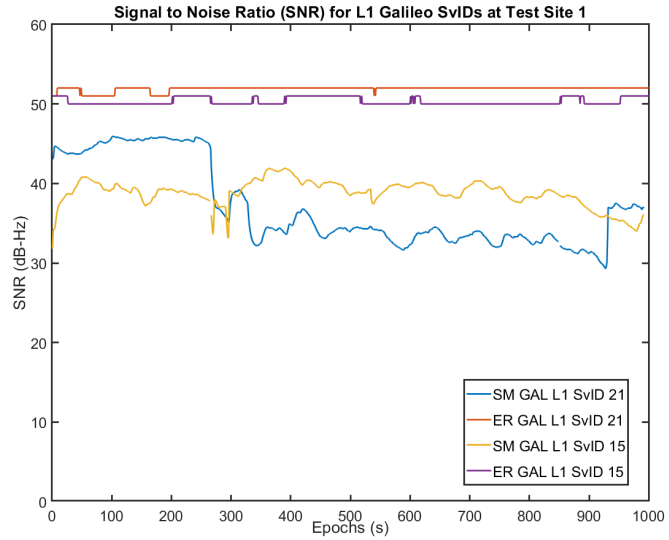

Fig. 11. Signal-to-Noise Ratio of selected L1 Galileo SvIDs for both receivers at Test Site 1

assessment of positioning errors obtained from PPP.

The PPP results, as shown in Fig. 12, illustrate the deviation patterns of both the Emlid Reach M2 (ER) and smartphone (SM) receivers from the reference solution. The 95% confidence intervals are highlighted to depict the precision and reliability of the PPP solutions obtained from RTKLIB and CSRS-PPP. As it can be seen in Fig. 12, the Emlid Reach M2 demonstrates exceptional performance, with its positional variations closely grouped around the reference point in both software applications. The 95% confidence intervals, represented as red and orange dashed circles for RTKLIB and CSRS-PPP, respectively, illustrate Emlid's great precision, with the smallest confidence radius recorded for CSRS-PPP (0.87 m). This emphasizes the device's profi-

		Test Site 1			
		SvID High		SvID Low	
		SM	ER	SM	ER
GPS L1	CP Available (%)	78.7	100	61.4	100
	No of Cycle Slips	95	5	70	5
GPS L5	CP Available (%)	61.6	100	75.1	100
	No of Cycle Slips	28	5	38	5
GAL L1	CP Available (%)	28.2	100	70.4	100
	No of Cycle Slips	57	5	104	5
GAL L5	CP Available (%)	75.3	100	87.9	100
	No of Cycle Slips	46	5	41	5

TABLE II
CARRIER PHASE (CP) AVAILABILITY AND CYCLE SLIPS FOR TEST SITE 1

ciency for high-precision applications, as evident also in the analysis of its raw measurements and its carrier tracking capabilities. In contrast, the smartphone exhibits greater positional variations, especially when analyzed with RTKLIB (blue dots), highlighting issues associated with noise and multipath effects due to its inferior GNSS antenna. When analyzed using CSRS-PPP (purple points), the smartphone data exhibits enhanced clustering, with a 95% confidence interval of 2.41 m, demonstrating the efficacy of CSRS-PPP's advanced correction algorithms in addressing the intrinsic limits of smartphone GNSS data. CSRS-PPP constantly surpasses RTKLIB in performance for both devices, providing reduced deviations and narrower confidence intervals, especially for the smartphone. Although the Emlid M2 exhibits superior precision, the smartphone findings processed with CSRS-PPP demonstrate its viability for applications necessitating intermediate accuracy. The findings indicate that smartphones, when combined with sophisticated post-processing methods, can function as a practical and accessible substitute for GNSS-based monitoring in situations requiring economical solutions. The dual-software methodology employed here highlights the significance of utilizing diverse algorithms to achieve general and dependable outcomes.

To assess the tropospheric delay estimation proficiency of the smartphones, the ZTD was derived from the raw GNSS data of both the Emlid Reach M2 and the Samsung Galaxy S24, utilizing the same software platforms, RTKLIB and CSRS-PPP. This was then compared with the EUREF product from the adjacent LIGN00ITA permanent GNSS station, with elevation differences between the testing site and the permanent station properly accounted for. Fig. 13 indicates that the Emlid Reach M2 outperformed the other tested devices in terms of ZTD accuracy, particularly when processed with CSRS-PPP. It produced a mean ZTD of 1862.47 mm, differing by less than 10 mm from the EUREF reference product, indicating strong agreement. In contrast, the same receiver processed with RTKLIB yielded a mean ZTD of 1832.16 mm, reflecting larger discrepancies likely due to differences in processing strategies and modeling approaches. The smartphone results followed a similar trend. When processed with CSRS-PPP, the mean ZTD was 1861.33 mm, showing close alignment with the benchmark, whereas RTKLIB processing led to a lower value of 1832.70 mm. These results highlight

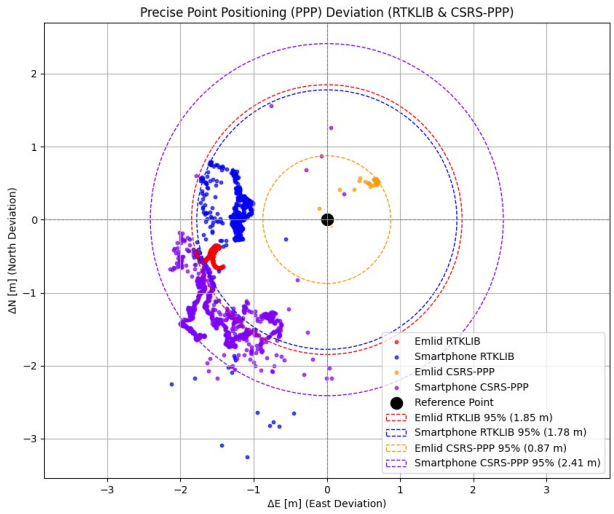

Fig. 12. Precise Point Positioning deviation comparison between smartphone Samsung Galaxy S24 and Emlid Reach M2 GNSS receiver processed by RTKLIB and CSRS-PPP.

the superior consistency and robustness of CSRS-PPP, which appears more effective at compensating for noise and device-related limitations in complex terrain.

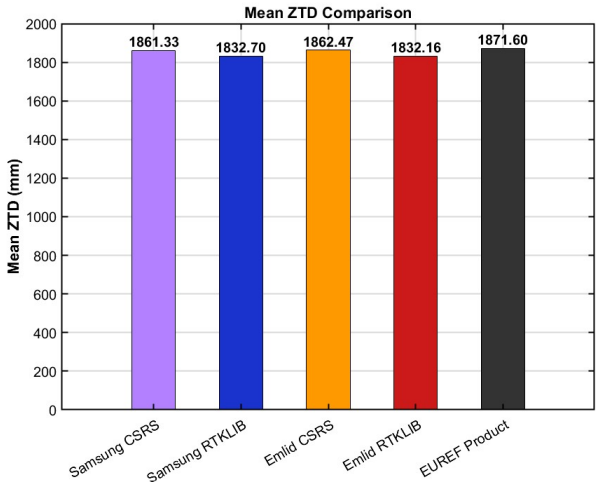

Fig. 13. ZTD estimation obtained (Mountainous, high altitude test site) compared with the EUREF product of LIGN00ITA master station located at Lignan, Italy.

B. Urban Environment Lower Altitude Tests

The skyplot of GPS and Galileo satellites on the 28th of January, 2025 is as shown in Fig. 14 and the combined GPS and Galileo satellite availability for both L1 and L5 frequencies can be seen in Fig. 15. It can be seen that the availability is slightly higher for both SM and ER than test site 1, which could be due to either the time of day or non-line-of-sight multipath contributions. However, the continuity of available measurements changes frequently across the 15-

minute test span for both the receivers, indicating the effects of an urban environment.

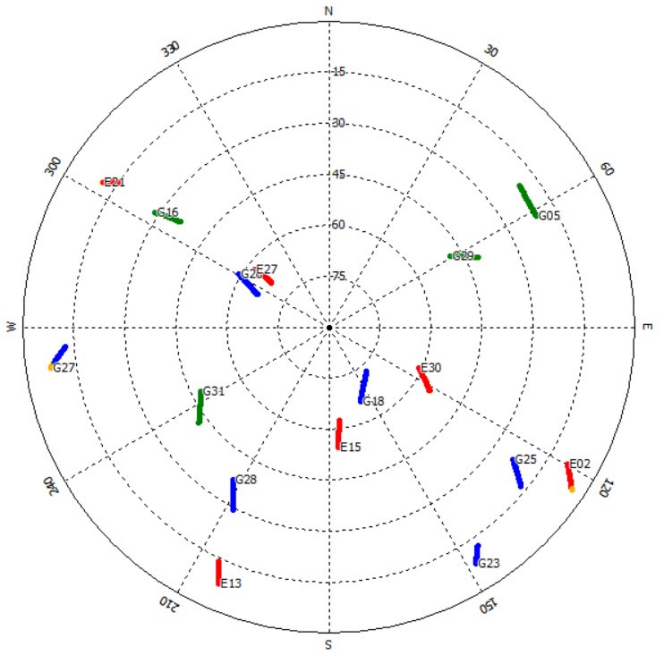

Fig. 14. Skyplot of Urban Low Altitude Test Site 2

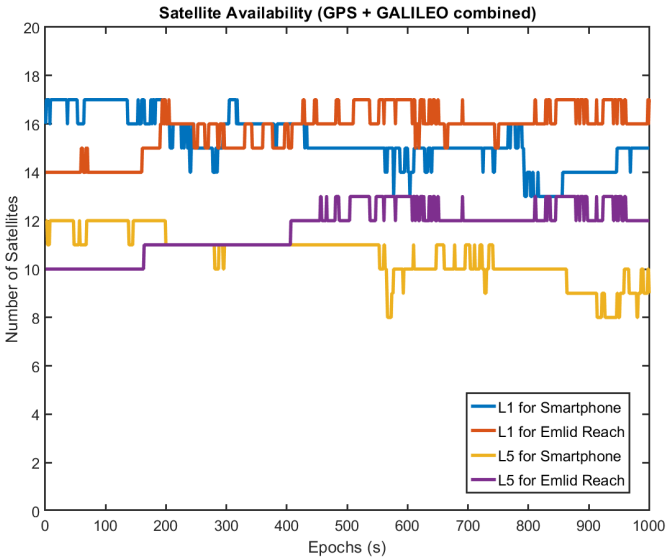

Fig. 15. Combined Satellite Availability at Test Site 2

1) Analysis of GNSS Raw Measurements: The higher and lower elevated satellites chosen to analyze are GPS SvID 18 and 25 and Galileo SvID 27 and 13, respectively.

The detrended pseudorange noise for GPS L1 and L5 can be seen in Fig. 16 and Fig. 17 respectively. There is no noticeable difference compared to test site 1 for the smartphone as the noise distribution is already in tens of meters. Similar behaviour is seen in the Galileo satellites, i.e., comparable

		Test Site 2			
		SvID High		SvID Low	
		SM	ER	SM	ER
GPS L1	CP Available (%)	92.4	100	54.2	100
	No of Cycle Slips	43	1	83	1
GPS L5	CP Available (%)	95.2	100	93.2	100
	No of Cycle Slips	31	1	38	1
GAL L1	CP Available (%)	89.6	100	51.4	100
	No of Cycle Slips	64	1	148	1
GAL L5	CP Available (%)	39.6	100	91.7	100
	No of Cycle Slips	57	1	47	1

TABLE III
CARRIER PHASE (CP) AVAILABILITY AND CYCLE SLIPS FOR TEST SITE 2

to test site 1. The disturbance seen around epoch 105 in all ER measurements occurs for the carrier phase measurements as well, leading to a cycle slip. This peculiar disturbance is similar to as seen in test site 1 and is undetectable in the SNR measurements. The SNR for the selected satellites at L1 frequency is plotted in Fig. 18, and the difference in quality between SM and ER is the same as previously seen. The ER multi-band antenna shows strong signal reception and interference resistance, albeit a bit worse than the previous test. L5 Signal-to-Noise Ratio values also show similar behaviour.

Table. III highlights the non-reliable nature of carrier phase measurements in the smartphone, as even with availability over 90% in most cases, there are small discontinuities in the measurements. Conversely, the ER multi-band antenna and receiver perform excellently in tracking the carrier phase, bar the one disturbance at epoch 105.

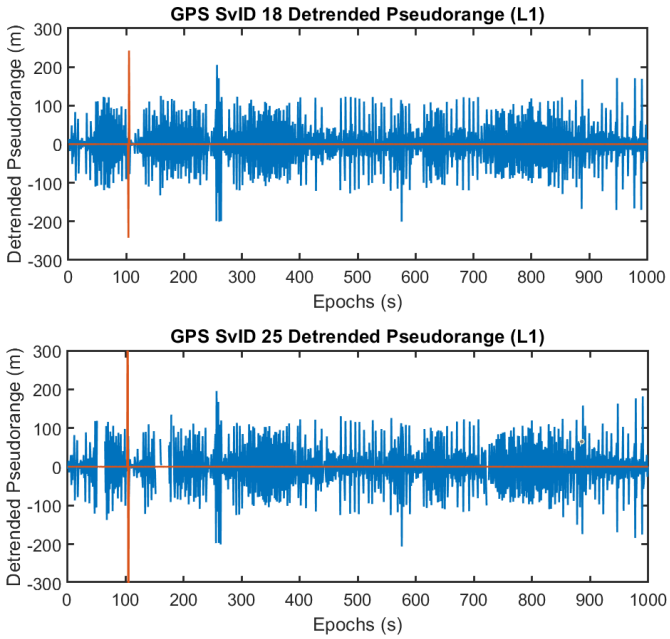

Fig. 16. GPS L1 Code Pseudorange Comparison for Test Site 2

2) Post Processed Positioning and ZTD Estimation Performances: The raw observation analysis in the urban area displayed features similar to those in the mountainous location,

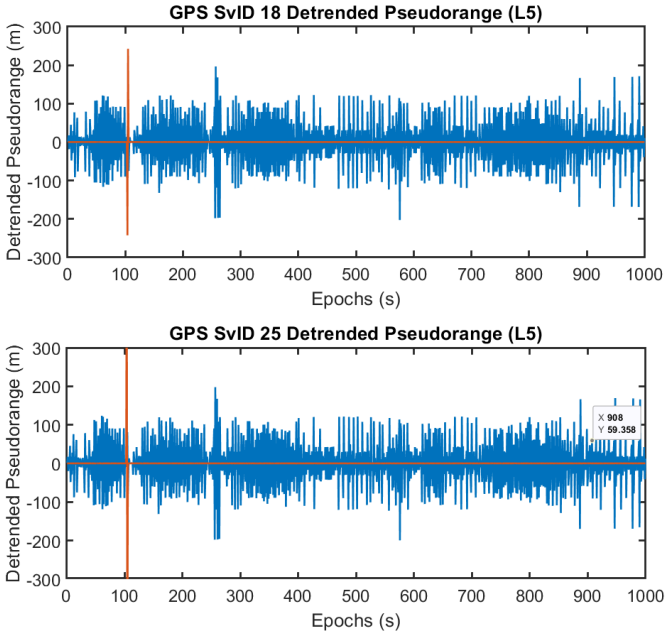

Fig. 17. GPS L5 Code Pseudorange Comparison for Test Site 2

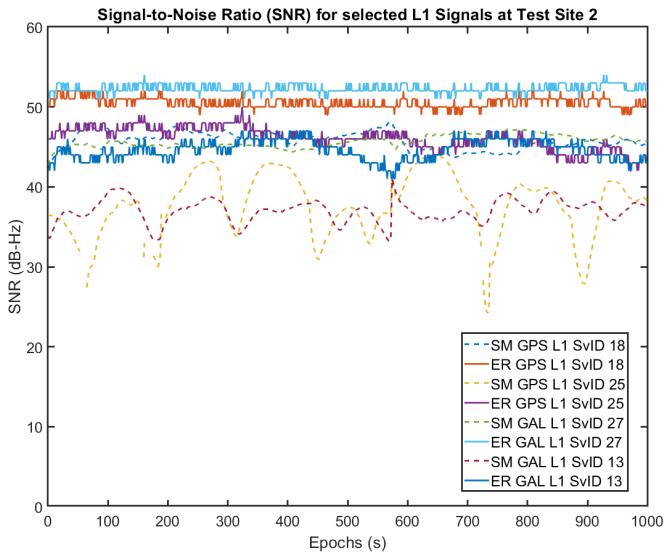

Fig. 18. Signal-to-Noise Ratio of selected L1 SvIDs for both receivers and constellations at Test Site 2

and the PPP results indicated similar behavior in both contexts. As a result, the investigation in the urban environment concentrated on the estimation of ZTD, as illustrated in Fig. 19. The bar chart presents the mean ZTD values derived from the Samsung Galaxy S24 smartphone and the Emlid Reach M2 receiver, processed using RTKLIB and CSRS-PPP software. These estimates are compared against the EUREF product from the TORI permanent GNSS station, which is located less than 300 meters from the test site, serving as the reference with a mean ZTD of 2287.50 mm. In the urban environment, the smartphone processed using RTKLIB achieved a ZTD difference of less than 2 mm compared to the EUREF reference, demonstrating exceptional performance despite the challenging conditions. This level of accuracy was not observed in the Emlid receiver or in the smartphone processed with CSRS-PPP, both of which exhibited greater deviations. The results suggest that, under certain conditions, open-source tools like RTKLIB, when properly configured, can deliver high-precision ZTD estimates from low-cost GNSS data even in urban settings.

The results demonstrate that smartphones, when processed appropriately, can achieve ZTD estimates with acceptable accuracy. In the mountainous environment, the smartphone processed with CSRS-PPP yielded a ZTD value within approximately 10 mm of the EUREF reference, indicating solid performance despite the challenging terrain. Notably, in the urban setting, the same smartphone processed with RTKLIB achieved exceptional agreement with the reference, showing a difference of less than 2 mm. These findings suggest that, under favorable conditions and with careful processing, smartphones can be a viable low-cost alternative for tropospheric delay estimation.

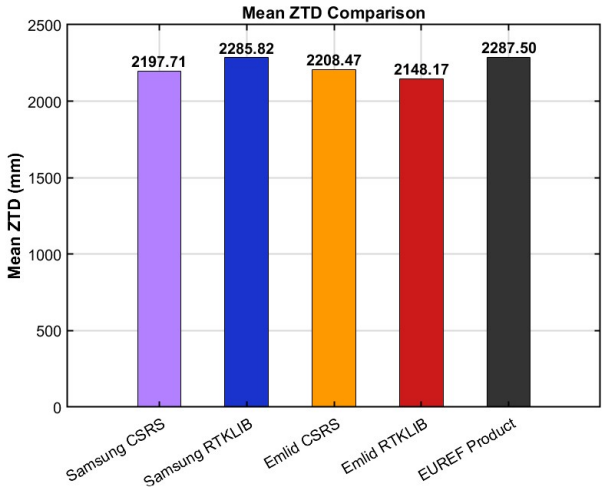

Fig. 19. ZTD estimation obtained (Urban environment lower altitude test site) compared with the EUREF product of TORI master station located at the rooftop of Politecnico di Torino, Italy.

IV. Conclusion

This preliminary research concludes that smartphones are viable for atmospheric monitoring, especially in estimating ZTD in a static scenario. This is despite the carrier phase measurements of the last smartphone models being unreliable, as found in this work and in the literature review. The findings indicate that smartphones, when processed appropriately, can still deliver ZTD estimates with acceptable accuracy. Specifically, in the mountainous environment, the smartphone processed with CSRS-PPP achieved a ZTD value within approximately 10 mm of the EUREF reference, while on a rooftop in an urban environment, the same smartphone processed with RTKLIB showed a difference of less than 2

mm, demonstrating strong agreement under favorable conditions. These results highlight the potential of smartphones as economical and accessible tools for atmospheric research. Furthermore, regarding positioning accuracy and ZTD estimation, smartphones demonstrate significant potential, indicating their viability as economical and easily accessible instruments for atmospheric research. However, further studies are necessary, involving a broader range of scenarios and extended data collection with a variety of modern smartphone GNSS chipsets, to fully validate these findings and assess their applicability to more demanding atmospheric monitoring tasks.

ACKNOWLEDGMENT

This study was carried out within the Space It Up project funded by the Italian Space Agency, ASI, and the Ministry of University and Research, MUR, under contract n. 2024-5-E.0 - CUP n. I53D24000060005.

REFERENCES

[1] International GNSS Service (IGS), "International GNSS Service (IGS),". Available: https://igs.org/. Accessed: Jan. 30, 2024.

[2] EPN Central Bureau, "EUREF Permanent Network Central Bureau (EPN CB)," [Online]. Available: https://www.epncb.oma.be/. Accessed: Nov. 25, 2024.

[3] SPIN3 GNSS, "Servizio di Posizionamento Interregionale GNSS," [Online]. Available: https://www.spingnss.it/. Accessed: Nov. 25, 2024.

[4] A. Krietemeyer, M.-C. Ten Veldhuis, H. Van der Marel, E. Realini, and N. Van de Giesen, "Potential of cost-efficient single frequency GNSS receivers for water vapor monitoring," *Remote Sens.-Basel*, vol. 10, p. 1493, 2018. [Online]. Available: https://doi.org/10.3390/rs10091493.

[5] K. Stępniak and J. Paziewski, "On the quality of tropospheric estimates from low-cost GNSS receiver data processing," *Measurement*, vol. 198, art. no. 111350, 2022. [Online]. Available: https://doi.org/10.1016/j.measurement.2022.111350

[6] A. Krietemeyer, H. van der Marel, N. van de Giesen, and M.-C. ten Veldhuis, "High quality zenith tropospheric delay estimation using a low-cost dual-frequency receiver and relative antenna calibration," *Remote Sens.*, vol. 12, p. 1393, 2020. [Online]. Available: https://doi.org/10.3390/rs12091393.

[7] P. Dabove and M. Bagheri, "Enhancing Atmospheric Monitoring Capabilities: A Comparison of Low- and High-Cost GNSS Networks for Tropospheric Estimations," *Remote Sens.*, vol. 16, p. 2223, 2024. [Online]. Available: https://doi.org/10.3390/rs16122223.

[8] F. Zangenehnejad and Y. Gao, "GNSS smartphones positioning: advances, challenges, opportunities, and future perspectives," *Satell. Navig.*, vol. 2, art. no. 24, 2021. [Online]. Available: https://doi.org/10.1186/s43020-021-00054-y

[9] M. Filić and R. Filjar, "Smartphone GNSS positioning performance improvements through utilisation of Google location API," in *Proc. 41st Int. Conv. Inf. Commun. Technol., Electron. Microelectron. (MIPRO)*, Opatija, Croatia, 2018, pp. 0458-0461. [Online]. Available: https://doi.org/10.23919/MIPRO.2018.8400087.

[10] Q. Wu, M. Sun, C. Zhou, and P. Zhang, "Precise point positioning using dual-frequency GNSS observations on smartphone," *Sensors*, vol. 19, art. no. 2189, 2019. [Online]. Available: https://doi.org/10.3390/s19092189.

[11] Smith, Jamie, et al. "Mapping the ionosphere with millions of phones." *Nature*, 635.8038 (2024): 365-369.

[12] Pan, Yuanxin, et al. "Determination of high-precision tropospheric delays using crowdsourced smartphone GNSS data." *Atmospheric Measurement Techniques*, 17.14 (2024): 4303-4316.

[13] Pesyna, K. M., R. W. Heath, and T. E. Humphreys. "Accuracy in the palm of your hand: Centimeter positioning with a smartphone-quality GNSS antenna." *GPS World*, 26.2 (2015): 16-31.

[14] Li, Bofeng, et al. "Ambiguity resolution for smartphone GNSS precise positioning: effect factors and performance." *Journal of Geodesy*, 96.9 (2022): 63.

[15] Gogoi, Neil, et al. "A controlled-environment quality assessment of Android GNSS raw measurements." *Electronics*, vol. 8, no. 1, 2018, p. 5.

[16] Paziewski, Jacek, et al. "An analysis of multi-GNSS observations tracked by recent Android smartphones and smartphone-only relative positioning results." *Measurement*, 175 (2021): 109162.

[17] Bramanto, Brian, Irwan Gumilar, and Irma AN Kuswanti. "Assessment of GNSS observations and positioning performance from non-flagship Android smartphones." *Journal of Applied Geodesy*, 18.2 (2024): 189-209.

[18] Paziewski, Jacek. "Recent advances and perspectives for positioning and applications with smartphone GNSS observations." *Measurement Science and Technology*, 31.9 (2020): 091001.

[19] Dabove, Paolo, and Vincenzo Di Pietra. "Towards high accuracy GNSS real-time positioning with smartphones." *Advances in Space Research* 63.1 (2019): 94-102.

[20] A. Angrisano, M. Bagheri, G. Cappello, P. Dabove, S. Del Pizzo, S. Gaglione, C. Gioia, G. Portelli, and S. Troisi, "Analysis of HAS performance in pedestrian navigation with different grade devices," in *Proc. 37th Int. Tech. Meeting of the Satellite Division of The Institute of Navigation (ION GNSS+ 2024)*, Baltimore, MD, USA, Sep. 2024, pp. 2123-2135. [Online]. Available: https://doi.org/10.33012/2024.19785.

[21] Riley, Stuart, Will Lentz, and Adam Clare. "On the path to precision-observations with Android GNSS observables." *Proceedings of the 30th International Technical Meeting of The Satellite Division of The Institute of Navigation (ION GNSS+ 2017)*, 2017.